EurJIC European Journal of Inorganic Chemistry

ChemPubSoc Europe

FULL PAPER

DOI:10.1002/ejic.201300196

Lanthanide(III) Complexes of Diethylenetriaminepentaacetic Acid (DTPA)–Bisamide Derivatives as Potential Agents for Bimodal (Optical/Magnetic Resonance) Imaging

Elke Debroye,[a] Svetlana V. Eliseeva,[b,c] Sophie Laurent,[d] Luce Vander Elst,[d] Stéphane Petoud,[b] Robert N. Muller,[d,e] and Tatjana N. Parac-Vogt*[a]

Keywords: Lanthanides / Luminescence / Imaging agents / Relaxation

Diethylenetriaminepentaacetic acid (DTPA)–bisamide derivatives functionalized with *p*-toluidine, 6-aminocoumarin, 1-naphthalene methylamine and 4-ethynylaniline were synthesized and fully characterized by mass spectrometry, NMR spectroscopy, FTIR spectroscopy and elemental analysis. Ln^{III} complexes (Ln = Gd, Eu, Tb, Y) of the ligands DTPA–bis-*p*-toluidineamide (DTPA–BTolA), DTPA–bis-6-coumarinamide (DTPA–BCoumA), DTPA–bis-1-naphthylmethylamide (DTPA–BNaphA) and DTPA–bis-4-ethynylphenylamide (DTPA–BEthA) were prepared and studied for their bimodal magnetic resonance imaging/optical properties. Eu^{III} and Tb^{III} derivatives in aqueous solutions exhibit characteristic red and green emission, respectively, with quantum yields of 0.73 % for Eu^{III}–DTPA–BNaphA and 2.5 % for Tb^{III}–DTPA–BEthA. Ligand-centred photophysical properties of the Gd^{III} complexes were investigated to gain insight into energy-transfer processes that take place in these systems. The Gd^{III} complexes were also analyzed by nuclear magnetic relaxation dispersion (NMRD) techniques. The relaxivity (r_1) at 20 MHz and 310 K equals 4.1 $s^{-1}\,mM^{-1}$ for Gd–DTPA–BTolA, 5.1 $s^{-1}\,mM^{-1}$ for Gd–DTPA–BCoumA, 6.4 $s^{-1}\,mM^{-1}$ for Gd–DTPA–BNaphA and 5.7 $s^{-1}\,mM^{-1}$ for Gd–DTPA–BEthA. These values are higher than the value of 3.8 $s^{-1}\,mM^{-1}$ for Gd–DTPA (Magnevist). The improved relaxivity is due to the increase in the rotational tumbling time τ_R with a factor of 1.6 for Gd–DTPA–BTolA, 2.1 for Gd–DTPA–BCoumA, 3.1 for Gd–DTPA–BNaphA and 6.5 for Gd–DTPA–BEthA. In a 4 % human serum albumin solution, the apparent relaxivity at 20 MHz increases to values of 13.9 and 19.1 $s^{-1}\,mM^{-1}$ for Gd–DTPA–BNaphA and Gd–DTPA–BEthA, respectively. All these features assist the search for optimal bimodal optical and magnetic resonance imaging probes.

Introduction

Improving the contrast in magnetic resonance imaging (MRI) requires contrast agents that are sufficiently stable and water-soluble with large values of molar relaxivity. It is commonly known that diethylenetriaminepentaacetic acid (DTPA) leads to the formation of highly stable complexes with trivalent lanthanide ions in aqueous solutions. Among the lanthanides, gadolinium(III) is preferred for in vivo MR applications because of its high paramagnetic character, and several Gd^{III} complexes are in clinical use as they enhance the T_1 signal intensity to result in a positive contrast.[1] Despite the good spatial resolution and tissue penetration, the MRI technique suffers from a low sensitivity. Moreover, the relaxivity remarkably decreases as the magnetic field strengths increase. To achieve better magnetic properties, the molecular tumbling rate of the contrast agent can be decreased by applying different strategies. Several Gd^{III} chelates have been conjugated to macromolecular carriers such as linear polymers or dendrimers.[2] The incorporation of amphiphilic Gd^{III} complexes into slowly tumbling micelles or liposomes also led to higher proton relaxivities.[1c,3] The formation of supramolecular structures that contain several paramagnetic ions has also been explored.[4] A more accessible approach to restrict the rotational motion is a noncovalent interaction of the ligand with proteins, such as human serum albumin (HSA),[5] which is the most abundant protein in human blood serum. In recent years luminescent/MRI bimodal agents have been created by tak-

[a] Department of Chemistry, KULeuven,
Celestijnenlaan 200F, 3001 Heverlee, Belgium
Fax: +32-16-327992
E-mail: Tatjana.Vogt@chem.kuleuven.be
Homepage: http://chem.kuleuven.be/lbc
[b] Centre de Biophysique Moléculaire CNRS UPR 4301,
Rue Charles Sadron, 45071 Orléans Cedex 2, France
[c] Le STUDIUM Institute for Advanced Studies,
Orléans and Tours, France
[d] Department of General, Organic and Biomedical Chemistry,
University of Mons,
Place du Parc 23, 7000 Mons, Belgium
[e] Center for Microscopy and Molecular Imaging (CMMI),
6041 Gosselies, Belgium

Supporting information for this article is available on the WWW under http://dx.doi.org/10.1002/ejic.201300196.

ing advantage of the high sensitivity of optical imaging coupled with the high resolution of MRI. These agents were designed by attaching an organic dye[6] or a transition-metal complex[7] to a DTPA or 1,4,7,10-tetraazacyclododecane-1,4,7,10-tetraacetic acid (DOTA) scaffold. The two diagnostic features were also combined into supramolecular structures like liposomes[8] or nanoparticles.[9] Eu^{III} and Tb^{III} chelates based on a DTPA core triggered a great deal of interest in the design of luminescent lanthanide systems.[10] These lanthanides display a unique pattern of sharp emission bands and typically have long-lived luminescent excited states in the microsecond–millisecond range. Since the corresponding f–f transitions are characterized by low molar absorption coefficients, an aromatic chromophore will be attached to the DTPA moiety. In such a system, the chromophore will act as "antenna"/sensitizer by gathering excitation energy and transferring it to the coordinated lanthanide ion. A mixture of the paramagnetic Gd^{III} and luminescent Eu^{III}, Tb^{III} or Yb^{III} complexes offers an imaging agent suitable for a diagnostic procedure endowed with the high resolution of MRI and the high sensitivity of optical imaging.[11]

Most of the gadolinium chelates are charged salts under physiological conditions and cause a high osmolality in solution in combination with their proper counterions.[12] On the other hand, neutral DTPA *N*,*N*′′-bisamide derivatives lead to minimal osmolality and display a satisfying complex stability and water solubility.[13] For in vivo applications, though, it is important to consider the kinetic inertness of the complexes. Kinetic stability can be evaluated as the extent of transmetalation of the complex in the presence of Zn^{II} ions at pH 7.[14] The results obtained for the Gd–DTPA bisamide series show that the transmetalation process is markedly faster for all bisamide derivatives than for the parent compound. However, within the bisamide series, less extensive transmetalation occurs when the substituting groups are bulkier, thus indicating a favourable effect of steric hindrance against the transmetalation process.[14b,15] The double amide functionalization provides a higher molecular weight, whereas the rigidity of the compound is maintained. These factors play an important role in improving the relaxivity properties of the corresponding gadolinium complexes. Furthermore, the attachment of one or two (different) aromatic systems can provide an absorbing centre to capture the energy of incident light, acting as an antenna for a coordinated europium or terbium ion. Lanthanide complexes with numerous amide derivatives of DTPA with substituted coumaryl,[16] carbostyryl,[17] naphthyl, quinoxalinyl,[18] phenylethynyl[19] and bipyridine[20] moieties among many others have been investigated as luminescent probes. Nevertheless, it remains a challenge to find a system that combines both optimal magnetic and optical properties, which can act as a bimodal contrast agent. In this report, four different DTPA–bisamides functionalized with *p*-toluidine, 6-aminocoumarin, *N*-(1-naphthyl)methylamine and 4-ethynylaniline as well as their lanthanide(III) complexes are synthesized and fully characterized by mass spectrometry, NMR spectroscopy, FTIR spectroscopy and elemental analysis. The photophysical properties of Gd^{III}, Eu^{III} and Tb^{III} complexes in aqueous solutions have been investigated in detail and the impact of the nature of the ligands is discussed. To evaluate the potential of the Gd^{III} analogues as MRI agents, their relaxometric properties were comprehensively studied in water and in HSA-containing solutions.

Results and Discussion

Synthesis of Ligands and Complexes

The DTPA–bisamide derivatives were prepared according to a straightforward two-step synthetic procedure (Scheme 1). Diethylenetriaminepentaacetic acid was treated with acetic anhydride to form DTPA–bisanhydride. Four different aromatic amines were coupled to this DTPA skeleton, which led to a set of DTPA–bisamide derivatives.

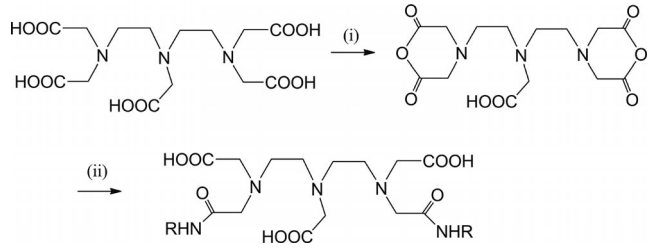

Scheme 1. General synthesis of DTPA–bisamide derivatives. Conditions: (i) acetic anhydride, pyridine, reflux; (ii) RNH_2, sodium ascorbate, anhydrous DMF, 60 °C.

The four synthesized ligands, DTPA–bis-*p*-toluidineamide (DTPA–BTolA), DTPA–bis-6-coumarinamide (DTPA–BCoumA), DTPA–bis-1-naphthylmethylamide (DTPA–BNaphA) and DTPA–bis-4-ethynylphenylamide (DTPA–BEthA), are depicted in Figure 1. All ligands were characterized by nuclear magnetic resonance spectroscopy (Figure S1 in the Supporting Information), mass spectrometry, elemental analysis and IR spectroscopy.

DTPA–BTolA was coordinated to paramagnetic Gd^{III}, luminescent Eu^{III} and Tb^{III} and diamagnetic Y^{III} in water in a mild acidic environment (pH ≈ 6). The lanthanide complexes of the other ligands were formed in pyridine according to the procedure by Kimpe et al.[21] The absence of free lanthanide ions was verified with the help of an arsenazo indicator solution.[22] Proton NMR spectroscopy of Y^{III}–DTPA–BCoumA and Y^{III}–DTPA–BNaphA shows a broadening and separation of the signals in the aliphatic region, which indicates the occurrence of several interconverting isomers due to the coordination of a lanthanide to DTPA derivatives (Figure S2 in the Supporting Information).[23] Positive-mode electrospray ionization mass spectrometry (ESI-MS) showed molecular peaks $[M + Na]^+$ and $[2M + Na]^+$, thus indicating the presence of fully complexed species with a 1:1 stoichiometry in solution (see Figure S3 in the Supporting Information and the Exp. Section). Infrared absorption data of all ligands show strong absorptions in the region around 1600 cm^{-1}, which correspond to the C=O

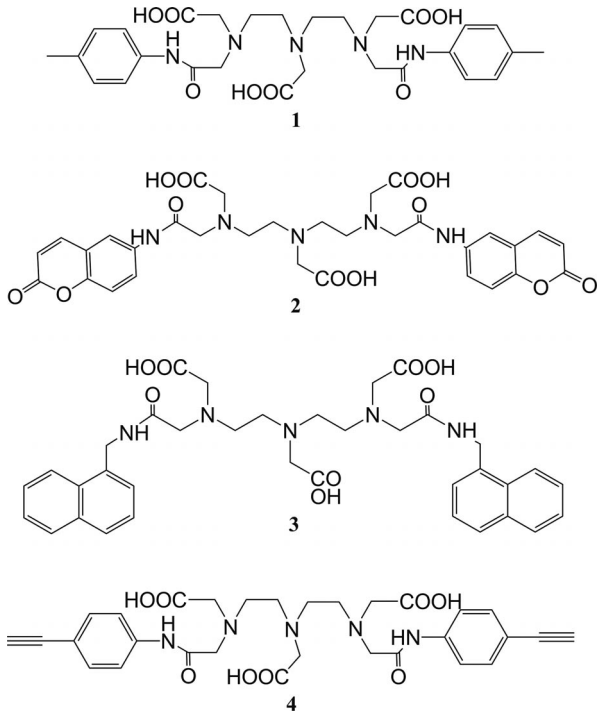

Figure 1. Synthesized DTPA–bisamide derivatives: DTPA–BTolA (**1**), DTPA–BCoumA (**2**), DTPA–BNaphA (**3**) and DTPA–BEthA (**4**).

free acid stretching modes. Shifts of 10 to 50 cm^{-1} towards lower wavenumbers were observed upon complexation, which suggests oxygen coordination to the lanthanide(III) ions. These findings are consistent with previous studies that have shown that DTPA–bisamide derivatives coordinate to trivalent lanthanide ions by three acetate oxygen atoms, three nitrogen atoms and two carbonyl oxygen atoms of the amide groups, whereas the ninth coordination site is occupied by a water molecule.[24] Owing to the strong coordinative properties of polyaminocarboxylates, the lanthanide complexes were found to be stable in water for several weeks at room temperature.

Photophysical Properties: Ligand-Centred Luminescence and Triplet States

All complexes displayed well-defined absorption bands (Figure 2 and Figure S4 in the Supporting Information), which can be attributed to the $\pi \rightarrow \pi^*$ transitions of the ligands. Absorption spectra are independent of the nature of the lanthanide ion, so only those of Gd^{III} complexes are discussed below. The Gd^{III} complex of DTPA–BTolA displayed an absorption maximum at 245 nm, whereas the Gd–DTPA–BCoumA complex showed an intense absorption band with a maximum at 245 nm and a shoulder at 275 nm. Moreover, a low-energy band at 323 nm can be seen for the latter. In comparison to parent coumarin with a maximum absorption wavelength of 274 nm,[25] the band is shifted towards higher energy upon derivatization with DTPA, thus forming an amide group at the 6-position. The absorption spectrum of Gd–DTPA–BNaphA showed an intense band at 219 nm and a less intense band at lower energy between 250 and 300 nm with three visible features located at 272, 282 and 291 nm. These represent the well-known $S_0 \rightarrow S_2$ transitions of naphthalene-based ligands.[26] Finally, for Gd–DTPA–BEthA, a maximum absorption can be seen at 263 nm, which corresponds to the phenylethynyl group of the ligand.[27]

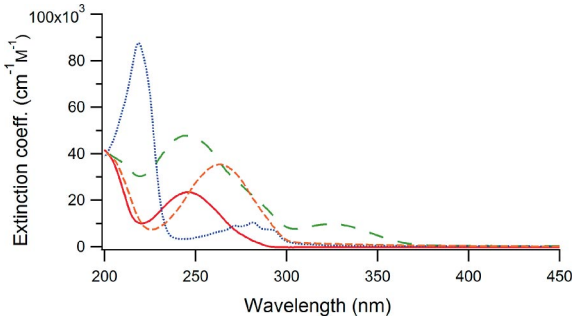

Figure 2. UV/Vis absorption spectra of Gd–DTPA–BTolA (Gd**1**) (solid line), Gd–DTPA–BCoumA (Gd**2**) (long-dashed line), Gd–DTPA–BNaphA (Gd**3**) (dotted line) and Gd–DTPA–BEthA (Gd**4**) (short-dashed line) in water (pH = 7.4, $c = 1 \times 10^{-5}$ M).

The photophysical properties of Gd^{III} complexes both at room temperature in aqueous solutions and at 77 K in a water/glycerol (9:1) mixture are summarized in Table 1. At 298 K, UV excitation into lower-energy bands results in ligand-centred broad-band emission that arises mainly from $^1\pi$–π^* states (Figure 3). At 77 K upon enforcing a time delay, the emission from the singlet state disappears to give rise to the triplet state $^3\pi$–π^* emission at lower energy.

Table 1. Ligand-centred photophysical properties.

	E_{S1}[a] [cm^{-1}]	E_{T1}[b] [cm^{-1}]	ΔE [cm^{-1}]	E_{T1}–$^5D_0$ [cm^{-1}]	E_{T1}–$^5D_4$ [cm^{-1}]
Gd**1**	26 670	20 325	6375	3025	–175
Gd**2**	26 385	21 460	4925	4160	960
Gd**3**	31 450	19 610	11 845	2310	–890
Gd**4**	27 000	22 000	5000	4700	1500

[a] Singlet-state energy, determined from the edge of the absorption spectra. [b] Triplet-state energy, determined as a 0–0 transition from the phosphorescence spectra of the Gd^{III} complexes.

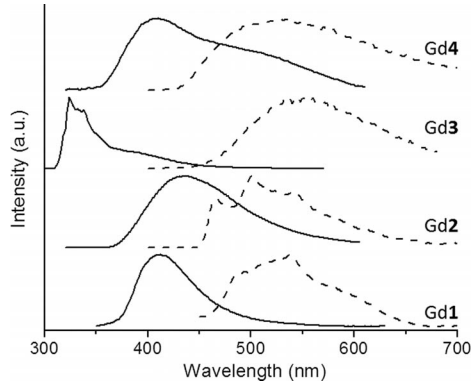

Figure 3. Normalized and corrected emission spectra of Gd^{III} complexes: luminescence at 295 K (H_2O, pH = 7.4, $c = 10^{-3}$ M, solid line) and phosphorescence at 77 K when a 100 μs delay was applied (H_2O/glycerol 9:1, $c = 10^{-3}$ M, dashed line).

Analysis of the data presented in Table 1 allows us to draw the following conclusions. (i) The difference between singlet and triplet states is quite ideal (≈5000 cm^{-1})[28] for efficient intersystem crossing for DTPA–BCoumA and DTPA–BEthA, whereas the ΔE value is too large for DTPA–BNaphA. (ii) Considering the energies of the triplet states and their comparison to the optimal values,[29] all ligands can serve as sensitizers of Eu^{III} luminescence with the maximum expected efficiency for Eu**3**. When it comes to Tb^{III}, E_{T1} of DTPA–BCoumA and DTPA–BEthA are too close to the $^5D_4$ level, thus making a back-energy-transfer process highly probable. Triplet-state energies of DTPA–BTolA and DTPA–BNaphA are lower than the resonance level of Tb^{III}, so they cannot be considered feeding levels for this ion.

Metal-Centred Luminescence

Under excitation at the proper wavelengths (280–330 nm), all Eu^{III} and Tb^{III} complexes except for Tb**3** display exclusively characteristic red and green emission bands due to $^5D_0 \rightarrow {}^7F_J$ (J = 0–4) and $^5D_4 \rightarrow {}^7F_J$ (J = 6–3) transitions, respectively (Figures 4, 5). Ligand-centred emission at lower wavelengths is absent, thus indicating an efficient ligand-to-lanthanide energy transfer. On the other hand, the emission spectrum of the Tb**3** complex is dominated by ligand emission centred at 325 nm with small sharp features in the range 450–650 nm typical for f–f transitions of the Tb^{III} ion. Such results can be expected if one takes into account that the triplet state of the DTPA–BNaphA is 890 cm^{-1} lower in energy than the resonant $^5D_4$ level of Tb^{III} (Table 1). Crystal-field splitting of the $^5D_0 \rightarrow {}^7F_J$ (J = 0–4) and $^5D_4 \rightarrow {}^7F_J$ (J = 6–3) transitions varies only slightly with the nature of the ligand, whereas relative intensities encounter some changes (Tables S1 and S2 in the Supporting Information). Considering Eu^{III} complexes, the relative integral intensity of the hypersensitive $^5D_0 \rightarrow {}^7F_2$ transition increases from 1.8 to 2.1 when going from Eu**4** to Eu**2** and further to 2.8 for Eu**1** and Eu**3**. The intensity of the highly forbidden $^5D_0 \rightarrow {}^7F_0$ transition is quite high (7–18% relative to $^5D_0 \rightarrow {}^7F_1$), which is typical for Eu^{III} occupying a site with C_s, C_n or C_{nv} symmetry. As far as Tb^{III} complexes are concerned, relative integral intensities vary within 20%, which is in agreement with the lower sensitivity of this ion to changes in the coordination environment than Eu^{III}.

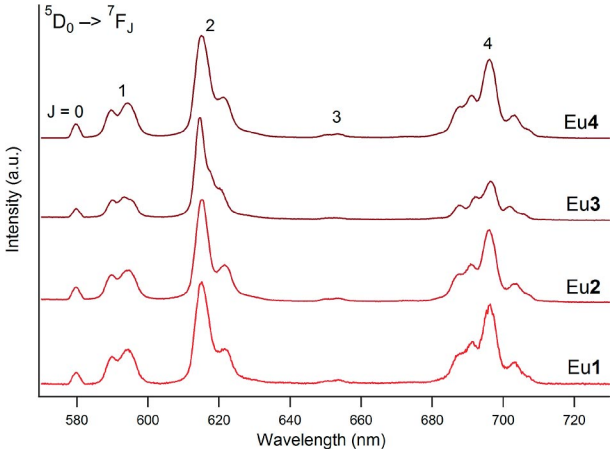

Figure 4. Bottom to top: Corrected and normalized emission spectra of Eu**1** (λ_{exc} = 280 nm), Eu**2** (λ_{exc} = 330 nm), Eu**3** (λ_{exc} = 292 nm) and Eu**4** (λ_{exc} = 290 nm) in water (pH = 7.4, $c = 10^{-5}$ M).

Luminescence decays of all Eu^{III} and Tb^{III} complexes in both H_2O and D_2O have been fitted by monoexponential equations to confirm the presence of only one luminescent lanthanide species in solution. Luminescence lifetimes in H_2O lie in the range of 0.54–0.57 ms for Eu^{III} and 1.49–1.58 ms for Tb^{III} complexes and are more or less independent of the nature of the ligand (Table 2). The τ_{H_2O} values are typical for the corresponding lanthanide complexes with DTPA–bisamide derivatives.[7a,20] In D_2O, luminescence lifetimes increase by a factor of approximately 4.7 and 2 for Eu^{III} and Tb^{III}, respectively. This is the result of less nonradiative deactivation induced by O–D vibrations than by O–H. The Eu^{III} luminescence lifetime decrease due to the presence of high-energy O–H vibrations is used for the determination of the number of coordinated water molecules q. For the sake of comparison in the case of Eu^{III}, two phenomenological equations developed for cyclen[30]

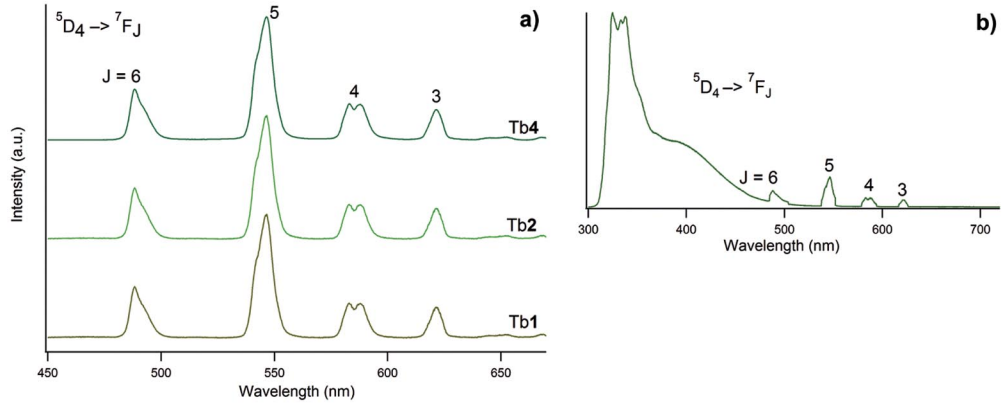

Figure 5. (a) Bottom to top: Corrected and normalized emission spectra of Tb**1** (λ_{exc} = 280 nm), Tb**2** (λ_{exc} = 330 nm) and Tb**4** (λ_{exc} = 290 nm) in water (pH = 7.4, $c = 10^{-5}$ M). (b) Corrected and normalized emission spectrum of Tb**3** (λ_{exc} = 292 nm).

and aminocarboxylate derivatives[31] have been considered [Equations (1) and (2)].

$$q_{Eu}\,(H_2O) = 1.2\,(\Delta k_{obsd.} - 0.25 - 1.2\,q^{NH} - 0.075\,q^{CONH}) \quad (1)$$

$$q_{Eu}\,(H_2O) = 1.11\,(\Delta k_{obsd.} - 0.31 - 0.44\,q^{OH} - 0.99\,q^{NH} - 0.075\,q^{CONH}) \quad (2)$$

Table 2. Photophysical data for the Eu^{III} and Tb^{III} complexes in water (pH 7.4, $c = 10^{-5}$ M) at 298 K.

	λ_{exc} [nm]	τ_{H_2O} [ms][a]	τ_{D_2O} [ms][a]	q_{H_2O}[b]
Eu**1**	280	0.54(1)	2.33(1)	1.2/1.1
Tb**1**	280	1.62(1)	3.09(1)	1.1
Eu**2**	330	0.56(1)	2.42(1)	1.2/1.1
Tb**2**	330	1.55(1)	3.11(1)	1.0
Eu**3**	292	0.57(1)	2.44(1)	1.1/1.0
Tb**3**	292	1.49(1)	3.07(1)	1.1
Eu**4**	290	0.57(1)	2.42(1)	1.1/1.0
Tb**4**	290	1.58(1)	3.13(1)	1.0
	τ_{rad} [ms][c]	Q^{Eu}_{Eu} [%][c]	Q^{L}_{Ln} [%][d]	η_{sens} [%][c]
Eu**1**	4.21	12.8	0.30	2.3
Tb**1**			0.62	
Eu**2**	5.38	10.4	0.64	6.2
Tb**2**			1.2	
Eu**3**	5.14	11.1	0.73[e]	6.6
Tb**3**			0.98[e]	
Eu**4**	5.58	10.2	0.55/0.58[e]	5.4/5.7[e]
Tb**4**			2.5/2.6[e]	

[a] Values of 2σ in parentheses. [b] Calculated using Equations (1) and (2) for Eu^{III} or Equation (3) for Tb^{III}. [c] Estimated relative errors: $\tau_{obsd.}$, ±2%; τ_{rad}, ±10%; Q^{Eu}_{Eu}, ±12%; Q^{L}_{Ln}, ±10%; η_{sens}, ±22%. [d] Quantum yield relative to quinine sulfate in 1 N H_2SO_4 unless stated otherwise. [e] Quantum yield relative to rhodamine 101 in EtOH.

For Tb^{III} the following phenomenological equation has been used [Equation (3)].[30]

$$q_{Tb}\,(H_2O) = 5.0\,(\Delta k_{obsd.} - 0.06) \quad (3)$$

In these equations, $\Delta k_{obsd.}$ represents the difference of the decay rate constants k_{H_2O} and k_{D_2O} or $1/\tau_{H_2O}$ and $1/\tau_{D_2O}$, and q^X stands for the number of OH, NH or CONH groups participating in lanthanide coordination. In the present case, only amide groups have been considered; $q^{CONH} = 2$. For Eu^{III} complexes, the values of q obtained using Equations (1) and (2) are in agreement [considering the accuracy of ±0.2–0.3 for Equation (1) and ±0.1 for Equation (2)] and lie in the range of 1.0 to 1.2 molecules. For Tb^{III} complexes, q is equal to 1.0–1.1. This is consistent with the eightfold lanthanide coordination provided by DTPA–bisamide derivatives, whereas the ninth coordination site is occupied by a water molecule in aqueous solutions.[24]

Although the nature of the ligand has no influence on the luminescence lifetimes, the quantum yields vary considerably and different trends can be observed for Eu^{III} and Tb^{III} complexes (Table 2). The quantum yields of Eu^{III} complexes determined under ligand excitation are very modest. They increase in the series Eu**1** < Eu**4** < Eu**2** < Eu**3** and reach 0.73% for the latter, which is quite in line with the predictions made according to the energy gap between E_{T1} and $^5D_0$ levels (Table 1). The low absorption coefficient of the f–f transitions does not allow us to measure intrinsic quantum yields, so they have been estimated on the basis of the ratio between the observed and radiative lifetimes according to Equation (4)

$$\frac{1}{\tau_{rad}} = A_{MD.0} \cdot n^3 \cdot \left(\frac{I_{tot}}{I_{MD}}\right) \quad (4a)$$

$$Q^{Eu}_{Eu} = \frac{\tau_{obsd.}}{\tau_{rad}} \quad (4b)$$

in which $A_{MD,0}$ is the Einstein coefficient equal to 14.65 s^{-1}; n the refractive index, which has been set equal to that of the neat solvent, $n_{H_2O} = 1.34$; and (I_{tot}/I_{MD}) the ratio of the total integrated $^5D_0 \rightarrow {}^7F_J$ emission (J = 0–4) to the integrated intensity of the $^5D_0 \rightarrow {}^7F_1$ magnetic dipole transition. The values of intrinsic quantum yields are in the range of 10–13%. The small variation of this parameter is somehow not surprising if one takes into account a similar coordination environment provided by the studied DTPA–bisamide derivatives. On the other hand, the sensitization efficiency defined by Equation (5)

$$\eta_{sens} = \frac{Q^{L}_{Eu}}{Q^{Eu}_{Eu}} \quad (5)$$

increases by 2.3–2.9 times for Eu**2**–Eu**4** complexes relative to Eu**1**, which reflects the trend observed for Q^{L}_{Eu}.

Tb^{III} luminescence quantum yields determined under ligand excitation follow a different trend than for Eu^{III} (Table 2). The maximum Q^{L}_{Tb} of 2.5% is observed for Tb**4**, whereas a value 2.1 times lower is found for Tb**2**. Quantum yields of Tb**3** and Tb**1** are even lower and equal to 0.98 and 0.62%, respectively. Tracing back to Table 1, one can conclude that contrary to the generally accepted triplet-to-lanthanide energy-transfer path, the singlet states of DTPA–BTolA and DTPA–BNaphA might play a significant role in the sensitization of characteristic Tb^{III} emission.

Relaxometric Studies: Longitudinal Relaxation Enhancement

The efficiency of an MRI contrast agent is usually measured by its water proton relaxivity (r_1), defined as the paramagnetic longitudinal relaxation rate induced by a 1 mM solution of Gd^{III}. It results mainly (i) from short-distance dipolar interactions between Gd^{III} and the water molecule coordinated to this ion and in exchange with bulk water (the so-called inner-sphere contribution) and (ii) from longer-distance dipolar interactions between the Gd^{III} complex and the water molecules diffusing in its close proximity (the outer-sphere interaction). The outer-sphere contribution is quite similar for all Gd complexes and depends on the distance of closest approach (d), the relative diffusion coefficient (D), the Gd^{III} electronic relaxation time at zero

field (τ_{S0}) and the correlation time that modulates the electronic relaxation (τ_V). The inner-sphere contribution is characterized by several parameters: r, the distance between the water protons and the paramagnetic centre; q, the number of water molecules in the first coordination sphere of Gd^{III}; τ_M, the residence time of the coordinated water molecule(s); τ_R, the rotational correlation time of the complex as well as τ_{SO} and τ_V.

The parameters d and r are usually set to 0.36 and 0.31 nm, respectively; q is equal to 1 for our complexes and D is equal to 3.3×10^{-9} $m^2 s^{-1}$ for Gd^{III} complexes with molecular weights that range from 500 to 1000.[32] Bisamide derivatives are expected to be characterized by a slow water exchange.[33] This was confirmed for the bisamide complex Gd–DTPA–BTolA as shown by the evolution of its relaxivity versus temperature at 20 MHz in Figure 6. For this complex, the water exchange is slower than for Gd^{III}–DTPA–bis-methylamide (Gd–DTPA–BMA), but the proton relaxivity at 37 °C is quite similar for the three complexes (Gd–DTPA, Gd–DTPA–BMA and Gd–DTPA–BTolA).

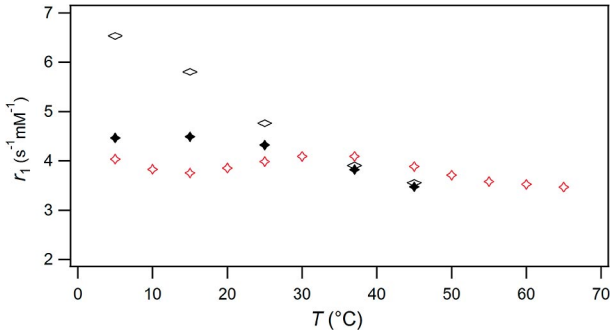

Figure 6. Evolution of the relaxivity of Gd–DTPA–BTolA (open diamonds) versus temperature in water at 20 MHz. The data of Gd–DTPA (rhombs) and Gd–DTPA–BMA (filled diamonds) are added for comparison.

Proton nuclear magnetic relaxation dispersion (NMRD) profiles represent the proton relaxivity as a function of the magnetic field. The NMRD profiles of Gd^{III}–DTPA–BTolA (1.0 mM), Gd^{III}–DTPA–BCoumA (0.81 mM), Gd^{III}–DTPA–BNaphA (1.06 mM) and Gd^{III}–DTPA–BEthA (0.84 mM) in water at 37 °C are shown in Figure 7.

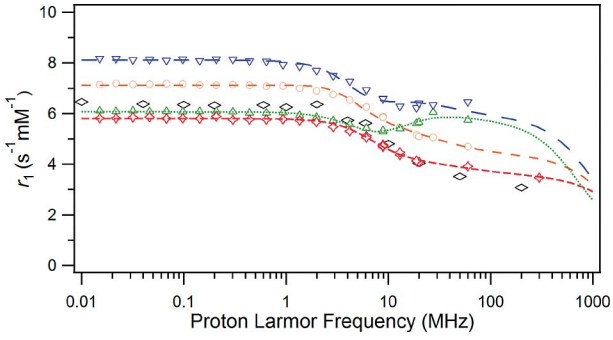

Figure 7. Proton NMRD profiles of Gd**1** (diamonds), Gd**2** (circles), Gd**3** (triangles down) and Gd**4** (triangles up) compared to Gd–DTPA (rhombs) in water at 37 °C. The dashed lines represent the fitted data.

Although Gd–DTPA–BCoumA and Gd–DTPA–BNaphA have a similar molecular weight, the relaxivity of the second one is remarkably larger. This effect could be due the formation of an aggregate through π stacking in the case of Gd–DTPA–BNaphA. Similarly, the maximum of the relaxivity obtained at high field (20–60 MHz) for Gd–DTPA–BEthA is probably due to intermolecular aggregation.

The inner- and outer-sphere contributions to the paramagnetic relaxation rate were taken into account during the theoretical adjustments of the NMRD profiles. Some parameters were fixed during this fitting procedure: q = 1; d = 0.36 nm; $D = 3.3 \times 10^{-9}$ $m^2 s^{-1}$ and r = 0.31 nm. The residence time of the coordinated water molecule (τ_M) was allowed to vary. The results of the theoretical fittings of the four different bisamide derivatives are shown in Table 3.

Table 3. Parameters obtained by the theoretical fitting of the proton NMRD data in water at 37 °C.

Gd^{III}–	DTPA[a]	BTolA	BCoumA	BNaphA	BEthA
d [nm][b]	–	0.36	0.36	0.36	0.36
D [10^{-9} $m^2 s^{-1}$][b]	–	3.3	3.3	3.3	3.3
r [nm][b]	–	0.31	0.31	0.31	0.31
τ_R [ps]	54 ± 1	87 ± 4	115 ± 2	169 ± 4	354 ± 92
τ_M [ns]	143	1340 ± 113	929 ± 29	600 ± 10	2520 ± 463
τ_{SO} [ps]	87 ± 3	65 ± 5	88 ± 1	90 ± 1	68 ± 6
τ_V [ps]	25 ± 3	18 ± 1	36 ± 2	32 ± 2	22 ± 1

[a] From the literature.[33] [b] Fixed values.

As expected for bisamide derivatives of Gd–DTPA, the τ_M values of Gd–DTPA–BTolA, Gd–DTPA–BCoumA and Gd–DTPA–BNaphA are high (600–1340 ns). The τ_R value of Gd–DTPA–BNaphA is 1.5 times larger than that of Gd–DTPA–BCoumA, thereby indicating some aggregation between the complexes. For Gd–DTPA–BEthA, the τ_R value obtained by the fitting is even larger (354 ps). However, the study of the relaxation rate of Gd–DTPA–BNaphA and Gd–DTPA–BEthA as a function of the concentration (between 0.1 and 1 mM and 0.15 and 2 mM, respectively) at 20 MHz does not show a clear deviation from linearity (as expected when Gd^{III} complexes form aggregates at high concentration). The formation of aggregates at concentrations lower than 0.1 mM could explain our results. The τ_M value obtained for Gd–DTPA–BEthA is larger than expected for a bisamide derivative. However, it should be noted that in such systems in which significant intermolecular interactions take place, the value of τ_M obtained from the fit of the NMRD profile is usually larger than expected.

Interaction with Human Serum Albumin (HSA)

The possible interaction of Gd–DTPA–BCoumA, Gd–DTPA–BNaphA and Gd–DTPA–BEthA with HSA was investigated (Figure 8). The enhancement of the apparent relaxivity of Gd–DTPA–BNaphA and Gd–DTPA–BEthA be-

tween 20 and 60 MHz clearly shows the presence of a significant interaction between HSA and these Gd^{III} complexes.

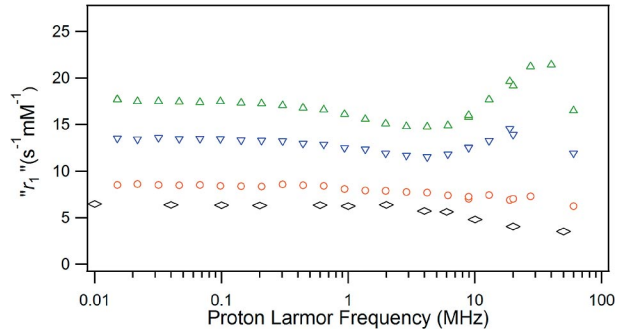

Figure 8. Apparent relaxivity of Gd–DTPA–BCoumA (0.81 mM; circles), Gd–DTPA–BNaphA (1.06 mM; downward triangles) and Gd–DTPA–BEthA (0.84 mM; upward triangles) in a 4% HSA solution relative to Gd–DTPA (1 mM; rhombs) in water at 37 °C.

To quantify the interaction, NMR spectroscopic titration experiments were performed for these complexes at 20 MHz and 37 °C in the presence of 4% HSA and various concentrations of the Gd^{III} complexes (Figure 9). The data of the titration experiments were fitted using Equation (6), in which P_o and L_o are the concentrations of the protein and contrast agent, respectively, r_1^B and r_1^F are the relaxivities of the bound and free complexes, respectively, N is the number of independent and equivalent binding sites and K_a is their association constant.

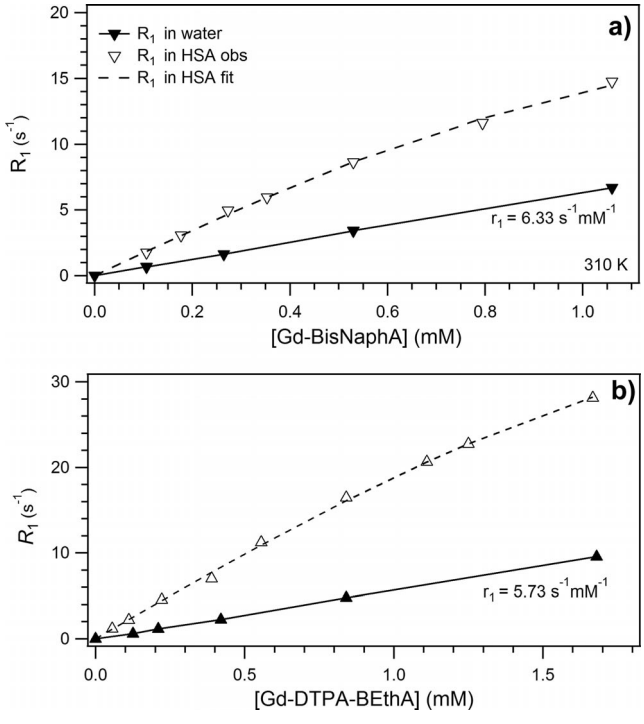

Figure 9. Proton longitudinal paramagnetic relaxation rate of (a) Gd–DTPA–BNaphA and (b) Gd–DTPA–BEthA as a function of the concentration in water (filled triangles) and in a 4% HSA solution (open triangles) at 37 °C.

$$R_1^{P}{}_{obs} = 1000L_0r_1^F + \frac{1000(r_1^B - r_1^F)\left[(NP_0 + L_0 + K_a^{-1}) - \sqrt{(NP_0 + L_0 + K_a^{-1})^2 - 4L_0NP_0}\right]}{2} \quad (6)$$

Despite the small number of points, the data were fitted to gain some insight into the strength of the interactions. From the fittings it seems that one binding site exists for Gd–DTPA–BNaphA with a K_a of about 1.5×10^4 M^{-1}, whereas 2 or 3 sites with a lower K_a would exist for Gd–DTPA–BEthA. Even if these values were to be considered a rough estimation, it can nevertheless be calculated that at the concentration of 1 mM Gd^{III} complex, more than 60 and 80% of Gd–DTPA–BNaphA and Gd–DPTA–BEthA, respectively, are bound to HSA.

Conclusion

A series of four different DTPA–bisamide derivatives with *p*-toluidine, 6-aminocoumarin, 1-naphthalene methylamine and 4-ethynylaniline moieties has been prepared and fully characterized. The DTPA units have been coordinated to paramagnetic Gd^{III}, luminescent Eu^{III} and Tb^{III} and diamagnetic Y^{III} for NMR spectroscopic studies. Photophysical data collected for Gd^{III}, Eu^{III} and Tb^{III} derivatives have shown an impact of the positions of both singlet and triplet states of the ligands with respect to the lanthanide emitting levels into the overall energy-transfer process. Quantum yield values of 0.73% for Eu–DTPA–BNaphA and 2.5% for Tb–DTPA–BEthA were obtained. These values are in fairly good agreement with the predictions that can be made according to the energy-gap law (E_{T1}–$^5D_0$) and (E_{T1}–$^5D_4$) (Table 1). However, if we take into account only the latter rule, one cannot explain the changes in the quantum yields for the other complexes. As for Eu^{III} complexes, the higher receiving energy levels $^5D_1$ and $^5D_2$ should be considered. Indeed, for Eu–DTPA–BCoumA, although (E_{T1}–$^5D_0$) = 4160 cm^{-1} is relatively large for an efficient energy transfer, the value of (E_{T1}–$^5D_1$) = 2390 cm^{-1} is quite ideal, which leads to a quantum yield of 0.64%. On the other hand, the triplet state of DTPA–BTolA (20325 cm^{-1}) is probably too high for the $^5D_0$ level but too close to the $^5D_1$ level to prevent back-energy transfer, which results in the lowest Q_{Eu}^L. The triplet-to-lanthanide path is generally considered to be the main energy-transfer process. However, sensitization of characteristic Tb^{III} emission with non-negligible quantum yields in Tb–DTPA–BTolA and Tb–DTPA–BNaphA has demonstrated that participation of the singlet states should not be neglected.[34] The intersystem crossing is to be taken into account: the low efficiency of this process for the Tb–DTPA–BNaphA complex is most probably responsible for the presence of a broad-band ligand-centred emission (Figure 5). The relaxivity r_1 at 20 MHz and 310 K equals 4.1 s^{-1} mM^{-1} for Gd–DTPA–BTolA, 5.1 s^{-1} mM^{-1} for Gd–DTPA–BCoumA, 6.4 s^{-1} mM^{-1} for Gd–DTPA–BNaphA and 5.7 s^{-1} mM^{-1} for Gd–DTPA–BEthA in comparison with a value of 3.8 s^{-1} mM^{-1} for Gd–DTPA (Magnevist). The improved relaxivity is due to the increase of the rota-

tional tumbling time τ_R with a factor 1.6 for Gd–DTPA–BTolA, 2.1 for Gd–DTPA–BCoumA, 3.1 for Gd–DTPA–BNaphA and 6.5 for Gd–DTPA–BEthA. In case of the latter two complexes, the large value of τ_R suggests aggregation by stacking of the aromatic ring systems. However, the study of the relaxation rate as a function of the concentration at 20 MHz does not show a clear deviation from linearity at increasing concentrations. In a 4% HSA solution, the apparent relaxivity at 20 MHz increases to values of 13.9 and 19.1 $s^{-1} mM^{-1}$ for Gd–DTPA–BNaphA and Gd–DTPA–BEthA, respectively. These chelates interact with the human blood serum protein to result in an increase of the rotational correlation time. These findings contribute to the formation of a platform for further studies that consider their bimodal optical and magnetic resonance imaging applications.

Experimental Section

Materials: Reagents and solvents were obtained from Sigma–Aldrich (Bornem, Belgium), Acros Organics (Geel, Belgium), Chem-Lab (Zedelgem, Belgium), Matrix Scientific (Columbia, USA) and BDH Prolabo (Leuven, Belgium) and were used without further purification. Gadolinium(III) and terbium(III) chloride hexahydrate were obtained from Alfa Aesar (Ward Hill, USA) and europium(III) and yttrium(III) chloride hexahydrate were obtained from Acros Organics (Geel, Belgium).

Instrumentation: Elemental analysis was performed with a CE Instruments EA-1110 elemental analyzer. ^1H and ^{13}C NMR spectra were recorded with a Bruker Avance 300 spectrometer (Bruker, Karlsruhe, Germany) operating at 300 MHz for ^1H and 75 MHz for ^{13}C, or with a Bruker Avance 400 spectrometer operating at 400 MHz for ^1H and 100 MHz for ^{13}C. IR spectra were measured with a Bruker Vertex 70 FTIR spectrometer (Bruker, Ettlingen, Germany). Mass spectra were obtained with a Thermo Finnigan LCQ Advantage mass spectrometer. Samples for the mass spectrometry were prepared by dissolving the product (2 mg) in methanol (1 mL), and then adding this solution (200 µL) to a water/methanol mixture (50:50, 800 µL). The resulting solution was injected at a flow rate of 5 µL min^{-1}. The metal contents were detected with a Varian 720-ES ICP optical emission spectrometer with reference to a Chem-Lab gadolinium standard solution (1000 µg mL^{-1}, 2–5% HNO_3). Absorption spectra were measured with a Varian Cary 5000 spectrophotometer on freshly prepared aqua solutions in quartz Suprasil cells (115F-QS) with an optical path length of 0.2 cm. Emission spectra and luminescence decays of Eu^{III} and Tb^{III} complexes were recorded with an Edinburgh Instruments FS920 steady-state spectrofluorimeter. This instrument was equipped with a 450 W xenon arc lamp, a high-energy microsecond flashlamp µF900H and an extended red-sensitive photomultiplier (185–1010 nm, Hamamatsu R 2658P). Emission spectra of Gd^{III} complexes at room and liquid-nitrogen temperature were measured with a Horiba-Jobin–Yvon Fluorolog 3 spectrofluorimeter. All spectra are corrected for the instrumental functions. Luminescence decays were determined under ligand excitation (280–330 nm) monitoring emission of $^5D_0 \rightarrow {}^7F_2$ and $^5D_4 \rightarrow {}^7F_5$ transitions for Eu^{III} and Tb^{III} complexes, respectively. Luminescence decays were analyzed using Edinburgh software; lifetimes are averages of at least three measurements. Quantum yields were determined by a comparative method with a standard reference; estimated experimental errors for quantum yield determination are ±10%. Quinine sulfate (Fluka) in 1 N sulfuric acid (Q = 54.6%) was used as a standard for the DTPA–BTolA, DTPA–BCoumA and DTPA–BEthA complexes and rhodamine 101 (Sigma) in ethanol (Q = 100%) was used as a standard for the DTPA–BNaphA and DTPA–BEthA complexes.[35] Solutions with a concentration of about 10^{-5} M were prepared to obtain an optical density lower than 0.05 at the excitation wavelength. The quantum yield values obtained using the two different standards for the Eu^{III}– and Tb^{III}–DTPA–BEthA complexes were the same within experimental error.

Proton Nuclear Magnetic Relaxation Dispersion (NMRD): Proton NMRD profiles were measured with a Stelar Spinmaster FFC, fast-field cycling NMR relaxometer [Stelar, Mede (PV), Italy] over a magnetic field strength range that extended from 0.24 mT to 0.7 T. Measurements were performed on samples (0.6 mL) contained in 10 mm (outside diameter) Pyrex tubes. Additional relaxation rates at 20, 60 and 300 MHz were obtained with a Minispec mq20, a Minispec mq60 and a Bruker Avance 300 spectrometer, respectively (Bruker, Karlsruhe, Germany). The proton NMRD curves were fitted using data-processing software,[36] including different theoretical models describing the nuclear relaxation phenomena (Minuit, CERN Library).[37]

Synthesis of DTPA–bisanhydride (DTPA–BA):[38] DTPA (3.93 g, 10 mmol, 1 equiv.), acetic anhydride (3.78 mL, 40 mmol, 4 equiv.) and pyridine (5 mL, 60 mmol, 6 equiv.) were combined and the reaction mixture was stirred at reflux for one hour. The resulting anhydride was removed by filtration and washed with acetic anhydride and dry diethyl ether. The cream-colored powder was then dried under vacuum at 40 °C until constant weight (yield: 2.97 g, 83%). ^1H NMR (300 MHz, [D$_6$]DMSO, 25 °C, SiMe$_4$): δ = 2.59 (t, 4 H, CH_2–CH_2–N–CH_2–CO_2H), 2.74 (t, 4 H, CH_2–CH_2–N–CH_2–CO_2H), 3.30 (s, 2 H, CH_2–CO_2H), 3.71 (s, 8 H, CH_2–CO–O–CO) ppm. ^{13}C NMR (75 MHz, [D$_6$]DMSO, 25 °C, SiMe$_4$): δ = 49.84 (CH_2–CH_2–N–CH_2–CO_2H), 51.63 (CH_2–CH_2–N–CH_2–CO_2H), 52.47 (CH_2–CO_2H), 54.88 (CH_2–CO–O–CO), 165.66 (CO–O–CO), 172.43 (CO_2H) ppm. ESI-MS (+ mode): m/z = calcd. 425.3 [M + 3Na]$^+$, found 423.9 [M + 3Na]$^+$. $C_{14}H_{19}N_3O_8$ (357.32): calcd. C 47.1, H 5.4, N 11.7; found C 46.9, H 5.5, N 11.5.

Synthesis of DTPA–BTolA (1):[21] *p*-Toluidine (0.27 g, 2.5 mmol, 2.5 equiv.) was added to a solution of DTPA–bisanhydride (0.36 g, 1 mmol, 1 equiv.) in dry DMF (30 mL). To avoid oxidation, a small amount of L-ascorbic acid sodium salt (50 mg, 0.25 mmol, 0.25 equiv.) was added and the reaction mixture was heated overnight at 60 °C under a nitrogen atmosphere. After evaporation of the solvent, the crude product was redissolved in methanol and precipitated by the dropwise addition of diethyl ether. The precipitate was removed by filtration and dried overnight under vacuum at 50 °C (yield: 0.43 g, 75%). ^1H NMR (400 MHz, CD_3OD, 25 °C, SiMe$_4$): δ = 2.26 (s, 6 H, Ph–CH_3), 3.21 (t, 4 H, CH_2–CH_2–N–CH_2–CO_2H), 3.43 (t, 4 H, CH_2–CH_2–N–CH_2–CO_2H), 3.56 (s, 4 H, N–CH_2–CO–NH), 3.58 (s, 4 H, N–CH_2–CO_2H), 3.90 (s, 2 H, N–CH_2–CO_2H), 7.18, 7.60 (d, 4 H, phenyl CH) ppm. ^{13}C NMR (100 MHz, CD_3OD, 25 °C, SiMe$_4$): δ = 19.50 (Ph–CH_3), 50.16 (CH_2–CH_2–N–CH_2–CO_2H), 53.43 (CH_2–CH_2–N–CH_2–CO_2H), 55.61, 58.33 (N–CH_2–CO), 120.24, 128.78 (phenyl CH), 133.69, 135.24 (phenyl C), 169.90 (CO–NH), 173.86 (CO_2H) ppm. IR: $\tilde{\nu}_{max}$ = 1612 (C=O free acid), 1516 (C=O amide) cm^{-1}. ESI-MS (+ mode): m/z: calcd. 594.6 [M + Na]$^+$, found 594.9 [M + Na]$^+$. $C_{28}H_{37}N_5O_8 \cdot H_2O$ (589.6): calcd. C 57.0, H 6.7, N 11.9; found C 57.3, H 6.7, N 12.1.

Synthesis of DTPA–BCoumA (2): 6-Aminocoumarin (0.40 g, 2.5 mmol, 2.5 equiv.) was added to a solution of DTPA–bisanhydride (0.36 g, 1 mmol, 1 equiv.) in dry DMF (30 mL). To avoid oxi-

dation, a small amount of L-ascorbic acid sodium salt (50 mg, 0.25 mmol, 0.25 equiv.) was added and the reaction mixture was heated overnight at 60 °C under a nitrogen atmosphere. After evaporation of the solvent, methanol was added, thereby resulting in an orange precipitated solution. The precipitate was removed by filtration and washed two times with methanol (20 mL) and two times with acetone (20 mL). The orange powder was heated at reflux in chloroform (120 mL) for three hours, removed by filtration and washed again twice with acetone (20 mL). The resulting yellow product was dried overnight under vacuum at 50 °C (yield: 0.54 g, 80%). ^{1}H NMR (300 MHz, [D$_5$]pyridine, 25 °C, SiMe$_4$): δ = 2.52 (t, 8 H, CH_2–CH_2–N), 3.20 (s, 10 H, N–CH_2–CO), 5.72, 6.51, 6.94, 7.40 (d, 2 H, coumarin CH), 7.72 (s, 2 H, coumarin C*H*) ppm. ^{13}C NMR (75 MHz, [D$_5$]pyridine, 25 °C, SiMe$_4$): δ = 51.75 (CH$_2$–*C*H$_2$–N–CH$_2$–CO$_2$H), 52.12 (*C*H$_2$–CH$_2$–N–CH$_2$–CO$_2$H), 55.59, 58.49 (N–*C*H$_2$–CO), 115.25, 115.36, 116.77, 117.60, 142.17 (coumarin *C*), 158.88 (coumarin *C*O), 169.00 (*C*O–NH), 172.25, 173.36 (*C*O$_2$H) ppm. IR: $\tilde{\nu}_{max}$ = 1574 (C=O free acid), 1495 (C=O amide) cm^{-1}. ESI-MS (+ mode): *m*/*z*: calcd. 680.6 [M + H]$^+$, 702.6 [M + Na]$^+$, found 681.2 [M + H]$^+$, 702.7 [M + Na]$^+$. $C_{32}H_{33}N_5O_{12}$ (679.64): calcd. C 56.5, H 4.9, N 10.3; found C 56.0, H 4.7, N 10.3.

Synthesis of DTPA–BNaphA (3): 1-Naphthalenemethylamine (0.39 g, 2.5 mmol, 2.5 equiv.) was added to a solution of DTPA–bisanhydride (0.36 g, 1 mmol, 1 equiv.) in dry DMF (30 mL). To avoid oxidation, a small amount of L-ascorbic acid sodium salt (50 mg, 0.25 mmol, 0.25 equiv.) was added and the reaction mixture was heated overnight at 60 °C under a nitrogen atmosphere. After evaporation of the solvent, the crude product was redissolved in methanol and precipitated by the dropwise addition of diethyl ether. The precipitate was removed by filtration and dried overnight under vacuum at 50 °C (yield: 0.58 g, 87%). ^{1}H NMR (300 MHz, CD$_3$OD, 25 °C, SiMe$_4$): δ = 2.98 (t, 4 H, CH$_2$–C*H*$_2$–N–CH$_2$–CO$_2$H), 3.19 (t, 4 H, C*H*$_2$–CH$_2$–N–CH$_2$–CO$_2$H), 3.37 (s, 4 H, N–C*H*$_2$–CO–NH), 3.40 (s, 4 H, N–C*H*$_2$–CO$_2$H), 3.65 (s, 2 H, N–C*H*$_2$–CO$_2$H), 4.76 (s, 4 H, C*H*$_2$–naphthyl), 7.38, 7.47 (m, 4 H, naphthyl C*H*), 7.73, 7.83, 7.98 (d, 2 H, naphthyl C*H*) ppm. ^{13}C NMR (75 MHz, CD$_3$OD, 25 °C, SiMe$_4$): δ = 41.96 (*C*H$_2$–naphthyl), 51.34 (CH$_2$–*C*H$_2$–N–CH$_2$–CO$_2$H), 54.18 (*C*H$_2$–CH$_2$–N–CH$_2$–CO$_2$H), 55.92, 57.10, 58.90 (N–*C*H$_2$–CO), 124.46, 126.52, 126.92, 127.13, 127.50, 129.20, 129.80 (naphthyl *C*H), 132.58, 134.97, 135.28 (naphthyl *C*), 170.47 (*C*O$_2$H), 172.93 (*C*O–NH), 175.11 (*C*O$_2$H) ppm. IR: $\tilde{\nu}_{max}$ = 1647 (C=O free acid), 1523 (C=O amide) cm^{-1}. ESI-MS (+ mode): *m*/*z*: calcd. 694.7 [M + Na]$^+$, found 695.8 [M + Na]$^+$. $C_{36}H_{41}N_5O_8$ (671.75): calcd. C 64.3, H 6.1, N 10.4; found C 64.1, H 5.8, N 10.1.

Synthesis of DTPA–BEthA (4): 4-Ethynylaniline (0.29 g, 2.5 mmol, 2.5 equiv.) was added to a solution of DTPA–bisanhydride (0.36 g, 1 mmol, 1 equiv.) in dry DMF (30 mL). To avoid oxidation, a small amount of L-ascorbic acid sodium salt (50 mg, 0.25 mmol, 0.25 equiv.) was added and the reaction mixture was heated overnight at 60 °C under nitrogen atmosphere. After evaporation of the solvent, the crude product was redissolved in methanol and precipitated by the dropwise addition of diethyl ether. The precipitate was removed by filtration and washed with ethyl ether. The orange powder was heated to reflux in chloroform (120 mL) for three hours, removed by filtration and washed again twice with acetone (20 mL). The product was dried overnight under vacuum at 50 °C (yield: 0.33 g, 56%). ^{1}H NMR (300 MHz, CD$_3$OD, 25 °C, SiMe$_4$): δ = 3.22 (t, 4 H, CH$_2$–C*H*$_2$–N–CH$_2$–CO$_2$H), 3.39 (s, 2 H, CH$_2$–CH$_2$–N–C*H*$_2$–CO$_2$H), 3.45 (t, 4 H, C*H*$_2$–CH$_2$–N–CH$_2$–CO$_2$H), 3.53 (s, 4 H, N–C*H*$_2$–CO$_2$H), 3.60 (s, 4 H, N–C*H*$_2$–CO–NH), 3.88 (s, 2 H, ethynyl C*H*), 7.32, 7.60 (d, 4 H, phenyl C*H*) ppm. ^{13}C NMR (75 MHz, CD$_3$OD, 25 °C, SiMe$_4$): δ = 51.63 (CH$_2$–*C*H$_2$–N–CH$_2$–CO$_2$H), 55.01 (*C*H$_2$–CH$_2$–N–CH$_2$–CO$_2$H), 56.22, 57.18, 59.98 (N–*C*H$_2$–CO), 79.49 (ethynyl *C*H), 84.31 (ethynyl *C*), 119.23 (phenyl *C*), 121.11, 133.51 (phenyl *C*H), 139.84 (phenyl *C*), 170.58 (*C*O$_2$H), 171.63 (*C*O–NH), 175.59 (*C*O$_2$H) ppm. IR: $\tilde{\nu}_{max}$ = 1599 (C=O free acid), 1512 (C=O amide) cm^{-1}. ESI-MS (+ mode): *m*/*z*: calcd. 614.6 [M + Na]$^+$, found 614.9 [M + Na]$^+$. $C_{30}H_{33}N_5O_8$ (591.62): calcd. C 60.9, H 5.6, N 11.8; found C 61.0, H 5.4, N 11.9.

Synthesis of Ln^{III}–DTPA–BTolA Complexes: The ligand (1 mmol) was dissolved in water (12 mL) and the acidity was adjusted to pH 6 with a sodium hydroxide solution. A solution of hydrated $LnCl_3$ salt (1.1 mmol) in H_2O (1 mL) was added. The mixture was brought to 70 °C for 3 h, after which the solvent was evaporated. The crude product was then heated at reflux in ethanol for one hour. The suspension was cooled to room temperature, then the complex was removed by filtration and dried under vacuum at 50 °C. The absence of free lanthanide ions was checked with an arsenazo indicator.[22]

^{157}Gd^{III}–DTPA–BTolA Gd1: Yield: 78%. IR: $\tilde{\nu}_{max}$ = 1599 (COO$^-$ asym. stretch), 1509 (amide II), 1396 (COO$^-$ sym. stretch) cm^{-1}. ESI-MS (+ mode): *m*/*z*: calcd. 748.8 [M + Na]$^+$, 1474.6 [2M + Na]$^+$, found 749.1 [M + Na]$^+$, 1474.5 [2M + Na]$^+$. UV/Vis: λ (ε, M^{-1} cm^{-1}) = 246 (23400) nm. **^{152}Eu^{III}–DTPA–BTolA:** Yield: 89%. IR: $\tilde{\nu}_{max}$ = 1597 (COO$^-$ asym. stretch), 1504 (amide II), 1394 (COO$^-$ sym. stretch) cm^{-1}. ESI-MS (+ mode): *m*/*z*: calcd. 743.6 [M + Na]$^+$, 1464.2 [2M + Na]$^+$, found 744.3 [M + Na]$^+$, 1464.3 [2M + Na]$^+$. UV/Vis: λ (ε, M^{-1} cm^{-1}) = 246 (22700) nm. **Tb^{III}–DTPA–BTolA:** Yield: 70%. IR: $\tilde{\nu}_{max}$ = 1598 (COO$^-$ asym. stretch), 1505 (amide II), 1393 (COO$^-$ sym. stretch) cm^{-1}. ESI-MS (+ mode): *m*/*z*: calcd. 750.5 [M + Na]$^+$, 1478 [2M + Na]$^+$, found 750.9 [M + Na]$^+$, 1477.8 [2M + Na]$^+$. UV/Vis: λ (ε, M^{-1} cm^{-1}) = 246 (23870) nm. **Y^{III}–DTPA–BTolA:** Yield: 95%. IR: $\tilde{\nu}_{max}$ = 1596 (COO$^-$ asym. stretch), 1504 (amide II), 1393 (COO$^-$ sym. stretch) cm^{-1}. ESI-MS (+ mode): *m*/*z*: calcd. 680.5 [M + Na]$^+$, 1338 [2M + Na]$^+$, found 680.6 [M + Na]$^+$, 1338.2 [2M + Na]$^+$.

Synthesis of Ln^{III}–DTPA–BCoumA, –BNaphA and –BEthA Complexes:[39] The ligand (1 mmol) was dissolved in pyridine (30 mL) and a solution of hydrated $LnCl_3$ salt (1.1 mmol) in H_2O (1 mL) was added. The mixture was brought to 70 °C for 3 h, after which the solvents were evaporated. The crude product was then heated at reflux in ethanol for one hour. The suspension was cooled to room temperature, then the complex was removed by filtration and dried under vacuum at 50 °C. The absence of free lanthanide ions was checked with an arsenazo indicator.

^{157}Gd^{III}–DTPA–BCoumA Gd2: Yield: 59%. IR: $\tilde{\nu}_{max}$ = 1563 (COO$^-$ asym. stretch), 1488 (amide II), 1435 (COO$^-$ sym. stretch) cm^{-1}. ESI-MS (+ mode): *m*/*z*: calcd. 856.9 [M + Na]$^+$, 1690.8 [2M + Na]$^+$, found 857.7 [M + Na]$^+$, 1691.4 [2M + Na]$^+$. UV/Vis: λ (ε, M^{-1} cm^{-1}) = 245 (47700), 324 (9800) nm. **^{152}Eu^{III}–DTPA–BCoumA:** Yield: 64%. IR: $\tilde{\nu}_{max}$ = 1562 (COO$^-$ asym. stretch), 1487 (amide II), 1436 (COO$^-$ sym. stretch) cm^{-1}. ESI-MS (+ mode): *m*/*z*: calcd. 851.6 [M + Na]$^+$, 1680.2 [2M + Na]$^+$, found 852.4 [M + Na]$^+$, 1679.5 [2M + Na]$^+$. UV/Vis: λ (ε, M^{-1} cm^{-1}) = 245 (49100), 324 (10050) nm. **Tb^{III}–DTPA–BCoumA:** Yield: 62%. IR: $\tilde{\nu}_{max}$ = 1562 (COO$^-$ asym. stretch), 1490 (amide II), 1436 (COO$^-$ sym. stretch) cm^{-1}. ESI-MS (+ mode): *m*/*z*: calcd. 858.5 [M + Na]$^+$, 1694.0 [2M + Na]$^+$, found 858.7 [M + Na]$^+$, 1693.6 [2M + Na]$^+$. UV/Vis: λ (ε, M^{-1} cm^{-1}) = 245 (47200), 324 (9650) nm. **Y^{III}–DTPA–BCoumA:** Yield: 59%. ^{1}H NMR (300 MHz, [D$_5$]pyridine, 25 °C, SiMe$_4$): δ = 2.55 (t, 8 H, CH_2–CH_2–N), 3.06 (s, 10 H, N–CH_2–CO), 5.76, 6.44, 6.58, 6.89 (d, 2 H, coumarin C*H*), 7.09 (s, 2 H, coumarin C*H*) ppm. IR: $\tilde{\nu}_{max}$ = 1563 (COO$^-$ asym. stretch), 1488 (amide II), 1437 (COO$^-$ sym. stretch) cm^{-1}. ESI-MS (+ mode): *m*/*z*: calcd. 788.5 [M

+ Na]$^+$, 1554.0 [2M + Na]$^+$, found 788.9 [M + Na]$^+$, 1554.3 [2M + Na]$^+$.

^{157}Gd^{III}–DTPA–BNaphA Gd3: Yield: 66%. IR: $\tilde{\nu}_{max}$ = 1593 (COO^- asym. stretch), 1512 (amide II), 1398 (COO^- sym. stretch) cm^{-1}. ESI-MS (+ mode): *m*/*z*: calcd. 849.0 [M + Na]$^+$, 1675.0 [2M + Na]$^+$, found 849.3 [M + Na]$^+$, 1676.7 [2M + Na]$^+$. UV/Vis: λ (ε, M^{-1} cm^{-1}) = 219 (87800), 272 (9050), 282 (10550), 291 (7500) nm. **^{152}Eu^{III}–DTPA–BNaphA:** Yield: 76%. IR: $\tilde{\nu}_{max}$ = 1589 (COO^- asym. stretch), 1510 (amide II), 1400 (COO^- sym. stretch) cm^{-1}. ESI-MS (+ mode): *m*/*z*: calcd. 843.7 [M + Na]$^+$, 1664.4 [2M + Na]$^+$, found 844.8 [M + Na]$^+$, 1665.6 [2M + Na]$^+$. UV/Vis: λ (ε, M^{-1} cm^{-1}) = 219 (93450), 272 (9600), 282 (11100), 291 (7850) nm. **Tb^{III}–DTPA–BNaphA:** Yield: 67%. IR: $\tilde{\nu}_{max}$ = 1591 (COO^- asym. stretch), 1514 (amide II), 1398 (COO^- sym. stretch) cm^{-1}. ESI-MS (+ mode): *m*/*z*: calcd. 850.6 [M + Na]$^+$, 1678.2 [2M + Na]$^+$, found 850.9 [M + Na]$^+$, 1678.0 [2M + Na]$^+$. UV/Vis: λ (ε, M^{-1} cm^{-1}) = 219 (89600), 272 (9300), 282 (10700), 291 (7650) nm. **Y^{III}–DTPA–BNaphA:** Yield: 80%. ^{1}H NMR (300 MHz, CD_3OD, 25 °C, $SiMe_4$): δ = 1.87 (t, 4 H, CH_2–C*H*$_2$–N–CH_2–CO_2^-), 2.09 (t, 4 H, C*H*$_2$–CH_2–N–CH_2–CO_2^-), 2.49 (s, 2 H, N–C*H*$_2$–CO_2^-), 2.91 (s, 4 H, N–C*H*$_2$–CO–NH), 2.98 (s, 4 H, N–C*H*$_2$–CO_2^-), 4.63 (s, 4 H, C*H*$_2$–naphthyl), 7.29, 7.40 (m, 4 H, naphthyl C*H*), 7.64, 7.71, 7.83 (d, 2 H, naphthyl C*H*) ppm. IR: $\tilde{\nu}_{max}$ = 1593 (COO^- asym. stretch), 1512 (amide II), 1402 (COO^- sym. stretch) cm^{-1}. ESI-MS (+ mode): *m*/*z*: calcd. 780.6 [M + Na]$^+$, 1538.2 [2M + Na]$^+$, found 781.9 [M + Na]$^+$, 1538.7 [2M + Na]$^+$.

^{157}Gd^{III}–DTPA–BEthA Gd4: Yield: 50%. IR: $\tilde{\nu}_{max}$ = 1583 (COO^- asym. stretch), 1508 (amide II), 1396 (COO^- sym. stretch) cm^{-1}. ESI-MS (+ mode): *m*/*z*: calcd. 768.8 [M + Na]$^+$, 1514.6 [2M + Na]$^+$, found 769.1 [M + Na]$^+$, 1515.0 [2M + Na]$^+$. UV/Vis: λ (ε, M^{-1} cm^{-1}) = 263 (35380) nm. **^{152}Eu^{III}–DTPA–BEthA:** Yield: 59%. IR: $\tilde{\nu}_{max}$ = 1585 (COO^- asym. stretch), 1509 (amide II), 1395 (COO^- sym. stretch) cm^{-1}. ESI-MS (+ mode): *m*/*z*: calcd. 763.6 [M + Na]$^+$, 1504.2 [2M + Na]$^+$, found 763.9 [M + Na]$^+$. UV/Vis: λ (ε, M^{-1} cm^{-1}) = 263 (36100) nm. **Tb^{III}–DTPA–BEthA:** Yield: 42%. IR: $\tilde{\nu}_{max}$ = 1583 (COO^- asym. stretch), 1508 (amide II), 1394 (COO^- sym. stretch) cm^{-1}. ESI-MS (+ve mode): *m*/*z*: calcd. 770.5 [M + Na]$^+$, 1518.0 [2M + Na]$^+$, found 770.9 [M + Na]$^+$, 1517.8 [2M + Na]$^+$. UV/Vis: λ (ε, M^{-1} cm^{-1}) = 263 (37150) nm. **Y^{III}–DTPA–BEthA:** Yield: 29%. IR: $\tilde{\nu}_{max}$ = 1590 (COO^- asym. stretch), 1510 (amide II), 1398 (COO^- sym. stretch) cm^{-1}. ESI-MS (+ mode): *m*/*z*: calcd. 700.5 [M + Na]$^+$, 1378 [2M + Na]$^+$, found 699.7 [M + Na]$^+$, 1377.6 [2M + Na]$^+$.

Supporting Information (see footnote on the first page of this article): ^{1}H NMR spectra of ligands **1**–**4** (Figure S1), ^{1}H NMR spectra of DTPA–BCoumA and DTPA–BNaphA compared to their Y^{III} complexes (Figure S2), ESI mass spectra of the ^{152}Eu^{III} complexes (Figure S3), UV/Vis absorption spectra of Eu^{III} and Tb^{III} complexes (Figure S4), relative integral intensities of f–f transitions for Eu^{III} complexes (Table S1) and Tb^{III} complexes (Table S2).

Acknowledgments

E. D. and T. N. P. V. acknowledge the IWT Flanders (Belgium) and the FWO Flanders (project number G.0412.09) for financial support. S. V. E. was a visiting postdoctoral fellow of the FWO Flanders (project number G.0412.09) and now works at the Centre de Biophysique Moléculaire - CNRS in Orléans. S. V. E and S. P. thank La Ligue contre le Cancer and the French National Research Agency (ANR) (project number ANR-10-BLAN-1513). CHN microanalysis was performed by Mr. Dirk Henot. ESI-MS measurements were done by Mr. Dirk Henot and Mr. Bert Demarsin and ICP-OES measurements were performed by Ms. Elvira Vassilieva (Department of Earth and Environmental Sciences). Mr. Karel Duerinckx is acknowledged for his help with the NMR spectroscopy measurements. S. L., L. V. E. and R. N. M. thank the ARC Programs of the French Community of Belgium, the Fonds National de la Recherche Scientifique (FNRS), the support and sponsorship provided by COST Actions (D38 and TD1004) and the EMIL program.

[1] a) P. Caravan, J. J. Ellison, T. J. McMurry, R. B. Lauffer, *Chem. Rev.* **1999**, *99*, 2293–2352; b) P. Hermann, J. Kotek, V. Kubicek, I. Lukes, *Dalton Trans.* **2008**, 3027–3047; c) A. Accardo, D. Tesauro, L. Aloj, C. Pedone, G. Morelli, *Coord. Chem. Rev.* **2009**, *253*, 2193–2213; d) S. Viswanathan, Z. Kovacs, K. N. Green, S. J. Ratnakar, A. D. Sherry, *Chem. Rev.* **2010**, *110*, 2960–3018.

[2] a) Y. Li, M. Beija, S. Laurent, L. Vander Elst, R. N. Muller, H. T. T. Duong, A. B. Lowe, T. P. Davis, C. Boyer, *Macromolecules* **2012**, *45*, 4196–4204; b) P. Lebdušková, J. Kotek, P. Hermann, L. Vander Elst, R. N. Muller, I. Lukeš, J. A. Peters, *Bioconjugate Chem.* **2004**, *15*, 881–889; c) G. M. Nicolle, É. Tóth, H. Schmitt-Willich, B. Radüchel, A. E. Merbach, *Chem. Eur. J.* **2002**, *8*, 1040–1048; d) H. Kobayashi, M. W. Brechbiel, *Curr. Pharm. Biotechnol.* **2004**, *5*, 539–549; e) K. Luo, G. Liu, W. She, Q. Wang, G. Wang, B. He, H. Ai, Q. Gong, B. Song, Z. Gu, *Biomaterials* **2011**, *32*, 7951–7960; f) A. J. L. Villaraza, A. Bumb, M. W. Brechbiel, *Chem. Rev.* **2010**, *110*, 2921–2959.

[3] a) T. N. Parac-Vogt, K. Kimpe, S. Laurent, C. Piérart, L. Vander Elst, R. N. Muller, K. Binnemans, *Eur. J. Inorg. Chem.* **2004**, 3538–3543; b) E. Terreno, D. Delli Castelli, C. Cabella, W. Dastrù, A. Sanino, J. Stancanello, L. Tei, S. Aime, *Chem. Biodiversity* **2008**, *5*, 1901–1912; c) C. Vanasschen, N. Bouslimani, D. Thonon, J. F. Desreux, *Inorg. Chem.* **2011**, *50*, 8946–8958; d) S. Y. Jeong, H. J. Kim, B.-K. Kwak, H.-Y. Lee, H. Seong, B. C. Shin, S. H. Yuk, S.-J. Hwang, S. H. Cho, *Nanoscale Res. Lett.* **2010**, *5*, 1970–1976.

[4] a) T. N. Parac-Vogt, L. Vander Elst, K. Kimpe, S. Laurent, C. Burtea, F. Chen, R. Van Deun, Y. C. Ni, R. N. Muller, K. Binnemans, *Contrast Media Mol. Imaging* **2006**, *1*, 267–278; b) T. N. Parac-Vogt, A. Pacco, P. Nockemann, S. Laurent, R. N. Muller, M. Wickleder, G. Meyer, L. Vander Elst, K. Binnemans, *Chem. Eur. J.* **2006**, *12*, 204–210.

[5] a) P. Caravan, G. Parigi, J. M. Chasse, N. J. Cloutier, J. J. Ellison, R. B. Lauffer, C. Luchinat, S. A. McDermid, M. Spiller, T. J. McMurry, *Inorg. Chem.* **2007**, *46*, 6632–6639; b) T. Parac-Vogt, K. Kimpe, S. Laurent, L. Vander Elst, C. Burtea, F. Chen, R. N. Muller, Y. Ni, A. Verbruggen, K. Binnemans, *Chem. Eur. J.* **2005**, *11*, 3077–3086; c) P. Caravan, *Acc. Chem. Res.* **2009**, *42*, 851–862; d) C. Henoumont, V. Henrotte, S. Laurent, L. Vander Elst, R. N. Muller, *J. Inorg. Biochem.* **2008**, *102*, 721–730.

[6] a) J. Kuil, T. Buckle, H. Yuan, N. S. van den Berg, S. Oishi, N. Fujii, L. Josephson, F. W. B. van Leeuwen, *Bioconjugate Chem.* **2011**, *22*, 859–864; b) A. Keliris, T. Ziegler, R. Mishra, R. Pohmann, M. G. Sauer, K. Ugurbil, J. Engelmann, *Bioorg. Med. Chem.* **2011**, *19*, 2529–2540; c) W. Di, S. K. P. Velu, A. Lascialfari, C. Liu, N. Pinna, P. Arosio, Y. Sakka, W. Qin, *J. Mater. Chem.* **2012**, *22*, 20641–20648.

[7] a) G. Dehaen, P. Verwilst, S. V. Eliseeva, S. Laurent, L. Vander Elst, R. N. Muller, W. M. De Borggraeve, K. Binnemans, T. N. Parac-Vogt, *Inorg. Chem.* **2011**, *50*, 10005–10014; b) G. Dehaen, S. V. Eliseeva, P. Verwilst, S. Laurent, L. Vander Elst, R. N. Muller, W. De Borggraeve, K. Binnemans, T. N. Parac-Vogt, *Inorg. Chem.* **2012**, *51*, 8775–8783; c) G. Dehaen, S. V. Eliseeva, K. Kimpe, S. Laurent, L. Vander Elst, R. N. Muller, W. Dehaen, K. Binnemans, T. N. Parac-Vogt, *Chem. Eur. J.* **2012**, *18*, 293–302; d) E. Debroye, G. Dehaen, S. V. Eliseeva, S. Laurent, L. Vander Elst, R. N. Muller, K. Binnemans, T. N. Parac-Vogt, *Dalton Trans.* **2012**, *41*, 10549–

10556; e) T. Koullourou, L. Natrajan, H. Bhavsar, S. J. A. Pope, J. Feng, R. Kauppinen, J. Narvainen, R. Shaw, E. Scales, A. Kenwright, S. Faulkner, *J. Am. Chem. Soc.* **2008**, *130*, 2178–2179.

[8] a) S. J. Soenen, G. V. Velde, A. Ketkar-Atre, U. Himmelreich, M. De Cuyper, *Wiley Interdiscip. Rev. Nanomed. Nanobiotechnol.* **2011**, *3*, 197–211; b) N. Kamaly, T. Kalber, G. Kenny, J. Bell, M. Jorgensen, A. Miller, *Org. Biomol. Chem.* **2010**, *8*, 201–211.

[9] a) D. Bhattacharya, M. Das, D. Mishra, I. Banerjee, S. K. Sahu, T. K. Maiti, P. Pramanik, *Nanoscale* **2011**, *3*, 1653–1662; b) Y. Chen, H. Chen, S. Zhang, F. Chen, L. Zhang, J. Zhang, M. Zhu, H. Wu, L. Guo, J. Feng, J. Shi, *Adv. Funct. Mater.* **2011**, *21*, 270–278; c) W. J. Rieter, J. S. Kim, K. M. L. Taylor, H. An, W. Lin, T. Tarrant, W. Lin, *Angew. Chem.* **2007**, *119*, 3754; *Angew. Chem. Int. Ed.* **2007**, *46*, 3680–3682; d) P. Howes, M. Green, A. Bowers, D. Parker, G. Varma, M. Kallumadil, M. Hughes, A. Warley, A. Brain, R. Botnar, *J. Am. Chem. Soc.* **2010**, *132*, 9833–9842.

[10] a) P. R. Selvin, T. M. Rana, J. E. Hearst, *J. Am. Chem. Soc.* **1994**, *116*, 6029–6030; b) G. R. Choppin, D. R. Peterman, *Coord. Chem. Rev.* **1998**, *174*, 283–299.

[11] a) S. L. C. Pinho, H. Faneca, C. F. G. C. Geraldes, J. Rocha, L. D. Carlos, M.-H. Delville, *Eur. J. Inorg. Chem.* **2012**, 2828–2837; b) L. Pellegatti, J. Zhang, B. Drahos, S. Villette, F. Suzenet, G. Guillaumet, S. Petoud, E. Toth, *Chem. Commun.* **2008**, 6591–6593; c) G. Tallec, P. H. Fries, D. Imbert, M. Mazzanti, *Inorg. Chem.* **2011**, *50*, 7943–7945.

[12] a) K. W.-Y. Chan, W.-T. Wong, *Coord. Chem. Rev.* **2007**, *251*, 2428–2451; b) S. Aime, A. Barge, E. Gianolio, R. Pagliarin, L. Silengo, L. Tei, in *Molecular Imaging, Vol. 49* (Eds.: A. A. Bogdanov, K. Licha), Springer, Berlin Heidelberg, **2005**, pp. 99–121.

[13] a) A. U. R. Sankar, M. Yamasitha, K. Srinivasulu, N. Ozaki, T. Aoki, M. Fujie, K. Ogawa, S. Okada, M. Yamada, Y. Tanaka, M. Kimura, M. Toda, *Tetrahedron Lett.* **2010**, *51*, 2431–2433; b) Z. Sideratou, D. Tsiourvas, T. Theodossiou, M. Fardis, C. M. Paleos, *Bioorg. Med. Chem. Lett.* **2010**, *20*, 4177–4181.

[14] a) M. F. Tweedle, J. J. Hagan, K. Kumar, S. Mantha, C. A. Chang, *Magn. Reson. Imaging* **1991**, *9*, 409–415; b) S. Laurent, L. Vander Elst, F. Copoix, R. N. Muller, *Invest. Radiol.* **2001**, *36*, 115.

[15] S. Laurent, F. Botteman, L. Vander Elst, R. N. Muller, *Eur. J. Inorg. Chem.* **2004**, 463–468.

[16] E. Heyduk, T. Heyduk, *Anal. Biochem.* **1997**, *248*, 216–227.

[17] M. S. Tremblay, M. Halim, D. Sames, *J. Am. Chem. Soc.* **2007**, *129*, 7570–7577.

[18] L. K. Chinen, K. P. Galen, K. T. Kuan, M. E. Dyszlewski, H. Ozaki, H. Sawai, R. S. Pandurangi, F. G. Jacobs, R. B. Dorshow, R. Rajagopalan, *J. Med. Chem.* **2008**, *51*, 957–962.

[19] A. D'Aléo, M. Allali, A. Picot, P. L. Baldeck, L. Toupet, C. Andraud, O. Maury, *C. R. Chim.* **2010**, *13*, 681–690.

[20] J. M. Couchet, J. Azéma, C. Galaup, C. Picard, *J. Lumin.* **2011**, *131*, 2735–2745.

[21] S. Laurent, T. N. Parac-Vogt, K. Kimpe, C. Thirifays, K. Binnemans, R. N. Muller, L. Vander Elst, *Eur. J. Inorg. Chem.* **2007**, 2061–2067.

[22] H. Onishi, K. Sekine, *Talanta* **1972**, *19*, 473–478.

[23] C. Geraldes, A. M. Urbano, M. A. Hoefnagel, J. A. Peters, *Inorg. Chem.* **1993**, *32*, 2426–2432.

[24] a) S. Aime, F. Benetollo, G. Bombieri, S. Colla, M. Fasano, S. Paoletti, *Inorg. Chim. Acta* **1997**, *254*, 63–70; b) Y.-M. Wang, Y.-J. Wang, R.-S. Sheu, G.-C. Liu, W.-C. Lin, J.-H. Liao, *Polyhedron* **1999**, *18*, 1147–1152.

[25] W. Jivaramonaikul, P. Rashatasakhon, S. Wanichwecharungruang, *Photochem. Photobiol. Sci.* **2010**, *9*, 1120–1125.

[26] a) G. Bergamini, P. Ceroni, M. Maestri, S.-K. Lee, J. van Heyst, F. Vögtle, *Inorg. Chim. Acta* **2007**, *360*, 1043–1051; b) I. Berlman, *Handbook of fluorescence spectra of aromatic molecules*, **1971**.

[27] R. Nandy, S. Sankararaman, *Beilstein J. Org. Chem.* **2010**, *6*, 992–1001.

[28] F. J. Steemers, W. Verboom, D. N. Reinhoudt, E. B. van der Tol, J. W. Verhoeven, *J. Am. Chem. Soc.* **1995**, *117*, 9408–9414.

[29] J.-C. Bünzli, S. Eliseeva, in: *Lanthanide Luminescence*, vol. 7 (Eds.: P. Hänninen, H. Härmä), Springer, Berlin Heidelberg, **2011**, pp. 1–45.

[30] A. Beeby, I. M. Clarkson, R. S. Dickins, S. Faulkner, D. Parker, L. Royle, A. S. de Sousa, J. A. Gareth Williams, M. Woods, *J. Chem. Soc. Perkin Trans. 2* **1999**, 493–504.

[31] R. M. Supkowski, W. D. Horrocks Jr., *Inorg. Chim. Acta* **2002**, *340*, 44–48.

[32] L. Vander Elst, A. Sessoye, S. Laurent, R. N. Muller, *Helv. Chim. Acta* **2005**, *88*, 574–587.

[33] a) F. Botteman, G. M. Nicolle, L. Vander Elst, S. Laurent, A. E. Merbach, R. N. Muller, *Eur. J. Inorg. Chem.* **2002**, 2686–2693; b) S. Laurent, L. Vander Elst, F. Botteman, R. Muller, *Eur. J. Inorg. Chem.* **2008**, 4369–4379.

[34] M. Kleinerman, *J. Chem. Phys.* **1969**, *51*, 2370.

[35] D. F. Eaton, *Pure Appl. Chem.* **1988**, *60*, 1107–1114.

[36] a) R. N. Muller, D. Declercq, P. Vallet, F. Giberto, B. Daminet, H. W. Fischer, F. Maton, Y. Van Haverbeke, in: *ESMRMB, 7th Annual Congress*, Proceedings of ESMRMB, 7th Annual Congress, Strasbourg, **1990**, p. 394; b) P. Vallet, PhD Dissertation, University of Mons-Hainaut, Belgium, **1992**.

[37] a) I. Solomon, *Phys. Rev.* **1955**, *99*, 559–565; b) N. Bloembergen, *J. Chem. Phys.* **1957**, *27*, 572–573; c) J. H. Freed, *J. Chem. Phys.* **1978**, *68*, 4034–4037.

[38] V. Montembault, J.-C. Soutif, J.-C. Brosse, *React. Funct. Polym.* **1996**, *29*, 29–39.

[39] K. Kimpe, T. N. Parac-Vogt, S. Laurent, C. Piérart, L. Vander Elst, R. N. Muller, K. Binnemans, *Eur. J. Inorg. Chem.* **2003**, 3021–3027.

Received: February 7, 2013
Published Online: March 28, 2013

